

Nonlinear Stochastic Density Steering via Gaussian Mixture Schrödinger Bridges and Multiple Linearizations

Mattia Mosso¹, George Rapakoulias¹, Yue Guan², Panagiotis Tsiotras³

¹ Graduate Student, School of Aerospace Engineering, Georgia Institute of Technology, Atlanta, GA, USA

² Postdoctoral Fellow, School of Aerospace Engineering, Georgia Institute of Technology, Atlanta, GA, USA

³ David and Andrew Lewis Chair and Professor, School of Aerospace Engineering, and Institute for Robotics and Intelligent Machines, Georgia Institute of Technology, Atlanta, GA, USA

I. Introduction

Controlling the stochastic evolution of a dynamical system between prescribed probability distributions is a fundamental problem at the intersection of optimal control, probability theory, and statistical mechanics [1]. A rigorous treatment of this problem forms the foundation of *Stochastic Optimal Control* (SOC). In the sequel, $x_t \in \mathbb{R}^n$ and $u_t \in \mathbb{R}^m$ denote the state and control input at time t , respectively. Let $w_t \in \mathbb{R}^p$ denote a p -dimensional Brownian motion process. The SOC problem is briefly summarized as

$$\inf_u V(t, x) = \mathbb{E} \left[\int_0^T L(s, x_s, u_s) ds + h(x_T) \right], \quad (1a)$$

$$\text{s.t. } dx_t = f_t(x_t) dt + B_t u_t dt + D_t dw_t, \quad (1b)$$

where L denotes the running cost, h is the terminal cost shaping the state distribution at the final time T , and $V(t, x)$ represents the expected cost-to-go. The state dynamics in (1b) are modeled as an Itô stochastic differential equation. Solving (1) amounts to solving the Hamilton–Jacobi–Bellman (HJB) equation, which, for general nonlinear SOC problems, is analytically intractable, while numerical methods are cumbersome due to the curse of dimensionality [2].

Furthermore, in many control problems, instead of implicitly controlling the final state distribution through the terminal cost $h(x_T)$, an explicit terminal distribution constraint is considered. This problem, which we refer to as a *density control problem*, has been studied extensively in the context of uncertainty control in autonomous systems [3–6], Schrödinger Bridge and optimal transport framework [7–10], and mean-field control theory [11–13]. While numerical solutions are expensive to obtain in a general setting, in the specific case where the boundary distributions are Gaussian, and the system dynamics are linear, efficient solutions can be obtained using semidefinite programming (SDP) through the *Optimal Covariance Steering* (OCS) framework [14–17] or even in closed form [18, 19].

While significant progress has been made in the field of covariance and density steering applied to complex aerospace stochastic planning problems [20–23], existing methods are largely restricted to linear (or locally linearized) dynamics. A major limitation emerges in regimes of large uncertainty. To this end, define the first-order Taylor expansion of the

dynamics around the mean $\mu(t) = \mathbb{E}[x(t)]$ as

$$f(x_t) = f(\mu_t) + \left. \frac{\partial f}{\partial x} \right|_{x_t=\mu_t} (x_t - \mu_t) + \mathcal{O}(\|x_t - \mu_t\|^2), \quad (2)$$

and let $\mathcal{R} \subseteq \mathbb{R}^n$ denote the region of validity of the above linear approximation. When the state distribution exhibits significant deviations from its assumed mean μ_t , the first-order approximation in (2) becomes unreliable, as a non-negligible portion of the probability mass may lie outside \mathcal{R} . Consequently, these approaches do not perfectly handle nonlinear systems with multi-modal uncertainty.

Recent advances in diffusion-based stochastic control [24, 25] demonstrate strong empirical performance, but they often lack explicit feedback synthesis and rigorous enforcement of terminal distribution constraints, which are critical in many applications. As a result, a computationally viable framework for stochastic, nonlinear, distribution-aware control with explicit terminal guarantees remains missing, in particular, in the context of trajectory optimization.

Contributions: We introduce a *multiple distribution-to-distribution linearization* framework that decomposes a nonlinear density steering problem into Gaussian-to-Gaussian OCS subproblems. We then show that each subproblem can be locally linearized and efficiently solved via semi-definite programming. We analyze our approach both theoretically and empirically for an Earth-to-Mars orbit-transfer problem, demonstrating improved performance over linearization-based baselines.

II. Preliminaries

This work builds upon two research areas in stochastic optimal control: covariance steering and the Schrödinger bridge problem (SBP). In this section, we provide a brief overview of these two research topics and summarize the key results relevant to our proposed approach.

A. Optimal Covariance Steering

The optimal covariance steering problem seeks a control policy that minimizes control effort while driving a stochastic time-varying dynamical system from a prescribed initial mean and covariance to a desired terminal mean and covariance, subject to the system dynamics and control constraints.

For continuous-time *linear* stochastic systems with Gaussian initial and terminal distributions, the OCS problem can be formulated as the following optimization problem:

$$\min_{u \in \mathcal{U}} \mathbb{E} \left[\int_0^T \|u_t\|^2 dt \right], \quad (3a)$$

$$\text{s.t. } dx_t = A_t x_t dt + B_t u_t dt + D_t dw_t, \quad (3b)$$

$$x_0 \sim \mathcal{N}(\mu_0, \Sigma_0), \quad x_T \sim \mathcal{N}(\mu_T, \Sigma_T). \quad (3c)$$

In the absence of chance constraints on the control and state, problem (3) admits an optimal solution in the form of the affine state-feedback law [14, 18]

$$u_t = K_t(x_t - \mu_t) + v_t, \quad (4)$$

where $K_t \in \mathbb{R}^{m \times n}$ governs the covariance dynamics, while $v_t \in \mathbb{R}^m$ is a feedforward term that steers the mean trajectory. Due to linearity, the mean- and covariance-steering problems are decoupled. The feedforward term v_t can be computed in closed form, or expressed as a quadratic program [17], and the feedback gain K_t can be computed via the semidefinite program [14, 17, 26] by solving

$$\min_{\Sigma_t, U_t, Y_t} \int_0^T \text{tr}(R_t Y_t) dt \quad (5a)$$

$$\text{s.t.} \quad \begin{bmatrix} \Sigma_t & U_t^\top \\ U_t & Y_t \end{bmatrix} \succeq 0, \quad \forall t \in [0, T]. \quad (5b)$$

$$\dot{\Sigma}_t = A_t \Sigma_t + \Sigma_t A_t^\top + B_t U_t + U_t^\top B_t^\top + D_t D_t^\top, \quad (5c)$$

$$\Sigma_0 = \Sigma_t|_{t=0}, \quad \Sigma_T = \Sigma_t|_{t=T} \quad (5d)$$

where $K_t = U_t \Sigma_t^{-1}$, and Y_t is a slack variable that equals $K_t \Sigma_t K_t^\top$ at optimality.

B. Nonlinear Covariance Steering via Linearization

When the system dynamics are nonlinear, the mean and covariance steering problems become coupled, rendering the problem significantly more challenging. Formally, the nonlinear version of the OCS problem is given by

$$\min_{u \in \mathcal{U}} \mathbb{E} \left[\int_0^T \|u_t\|^2 dt \right], \quad (6a)$$

$$\text{s.t.} \quad dx_t = f_t(x_t)dt + B_t u_t dt + D_t dw_t, \quad (6b)$$

$$x_0 \sim \mathcal{N}(\mu_0, \Sigma_0), \quad x_T \sim \mathcal{N}(\mu_T, \Sigma_T), \quad (6c)$$

where f_t is a state-dependent nonlinear drift function. We note that although we keep B_t and D_t state-independent in our analysis, a more general analysis in which they are also state-dependent can be easily carried out [20]. While analytical solutions to the nonlinear OCS problem remain open, several approaches have been developed to compute approximate solutions.

For example, [20] proposed the iterative Covariance Steering (iCS) approach, where the nonlinear problem is iteratively solved as a sequence of approximate linear covariance steering problems, leveraging the principle of successive convexification [27]. The iCS approach iterates between (i) propagating the nonlinear mean dynamics (6b) under the

current control law and (ii) linearizing the system about the resulting mean trajectory. The algorithm is initialized with an initial guess of the control law $\bar{u}_t^{(0)}$. At each iteration k , the control law $\bar{u}_t^{(k)}$ is used to propagate the nonlinear dynamics and obtain the mean trajectory $\bar{x}_t^{(k)}$. The nonlinear dynamics are then linearized around $(\bar{x}_t^{(k)}, \bar{u}_t^{(k)})$. Introducing the deviation variables $\tilde{x}_t = x_t - \bar{x}_t^{(k)}$ and $\tilde{u}_t = u_t - \bar{u}_t^{(k)}$ yields a local continuous-time linear stochastic system with additive noise of the form

$$d\tilde{x}_t \approx (A_t \tilde{x}_t + B_t \tilde{u}_t) dt + D_t dw_t, \quad (7a)$$

$$A_t = \left. \frac{\partial f_t}{\partial x} \right|_{x=\bar{x}_t^{(k)}}, \quad (7b)$$

where A_t denotes the Jacobian evaluated along the reference trajectory. The resulting linearized problem is solved via the SDP in (5), yielding an updated control $u_t^{(k+1)}$. This procedure is repeated until convergence. Observe that the resulting problem at each iteration is formulated as a convex optimization problem (5), which is solved to obtain the optimal feedforward v_t and feedback gain K_t , subject to the linearized dynamics.

C. Gaussian Mixture Schrödinger Bridge

Consider now a generalization of the linear OCS in (3) where, instead of Gaussian marginals, the initial and final boundary distributions are GMMs with N_0 and N_1 components, respectively. Then, the optimization problem is cast as follows

$$\min_{u \in \mathcal{U}} J_{\text{GMM}} \triangleq \mathbb{E} \left[\int_0^T \|u_t(x_t)\|^2 dt \right], \quad (8a)$$

$$\text{s.t. } dx_t = A_t x_t dt + B_t u_t dt + D_t dw_t, \quad (8b)$$

$$x_0 \sim \sum_{i=1}^{N_0} \alpha_0^i \mathcal{N}(\mu_0^i, \Sigma_0^i), \quad x_T \sim \sum_{j=1}^{N_1} \alpha_T^j \mathcal{N}(\mu_T^j, \Sigma_T^j). \quad (8c)$$

An approximation to the solution of (8) can be achieved following the method presented in [8]. Let $u_{t|ij}$ be the conditional policy that solves the (i, j) -OCS problem, i.e., an affine control law of the form (4), that steers the system (8b) from the i -th component of the initial Gaussian mixture to the j -th component of the terminal mixture, and let $\rho_{t|ij}$ be the resulting Gaussian density of the (i, j) -OCS problem. A feasible set of control laws for (8) is given by

$$u_t(x) = \sum_{i,j} u_{t|ij}(x) \frac{\rho_{t|ij}(x) \lambda_{ij}}{\sum_{i',j'} \rho_{t|i'j'}(x) \lambda_{i'j'}}, \quad (9)$$

where λ_{ij} is a set of positive weights, obtained through the linear program in (11) [8, Theorem 1], while the corresponding density of the state is

$$\rho_t = \sum_{ij} \lambda_{ij} \rho_{t|ij}. \quad (10)$$

The calculation of the component-level transport plan λ_{ij} is computed by solving

$$\min_{\lambda_{ij} \geq 0} J_{\text{OT}} \triangleq \sum_{i,j} \lambda_{ij} C_{ij}, \quad (11a)$$

$$\text{s.t.} \quad \sum_j \lambda_{ij} = \alpha_0^i, \quad \forall i = 1, \dots, N_0, \quad (11b)$$

$$\sum_i \lambda_{ij} = \alpha_T^j, \quad \forall j = 1, \dots, N_1, \quad (11c)$$

where C_{ij} is the cost of the (i, j) -OCS subproblem [8, Theorem 2]. Notice that the proposed weighting scheme prioritizes the conditional policies whose mean is closer to the value of x_t . This formulation incorporates the idea that each (i, j) reference policy is associated with a prior probability λ_{ij} induced by the optimal transport coupling, while the state x_t at time t has a known likelihood of being generated from the Gaussian component $\rho_{t|ij}$. Similar concepts have also been explored in discrete-time density control problems using GMMs [28–30].

D. Fokker-Planck-Kolmogorov Equation

Recall that the time evolution of the state distribution ρ_t governed by the controlled Itô SDE

$$dx_t = (f_t(x_t) + B_t u_t) dt + D_t dw_t \quad (12)$$

is described by the Fokker-Planck-Kolmogorov (FPK) equation [31],

$$\frac{\partial \rho_t}{\partial t} + \nabla \cdot [\rho_t (f_t + B_t u_t)] - \frac{1}{2} \text{tr}(D_t D_t^\top \nabla^2 \rho_t) = 0, \quad (13)$$

where $\nabla^2 \rho_t$ denotes the Hessian of the probability density. In our analysis, we use the FPK equation to show that a control law u_t , and a candidate density ρ_t are consistent, that is, if u_t is applied to the SDE (12), the resulting density will be ρ_t .

III. Nonlinear Density Steering

In this section, we extend the techniques presented in Section II to approximate the nonlinear density steering problem. While, in general, a final distribution constraint increases the complexity of solving an SOC problem, in the proposed formulation, we exploit this additional structure to construct a set of reference linearizations that synthesize a

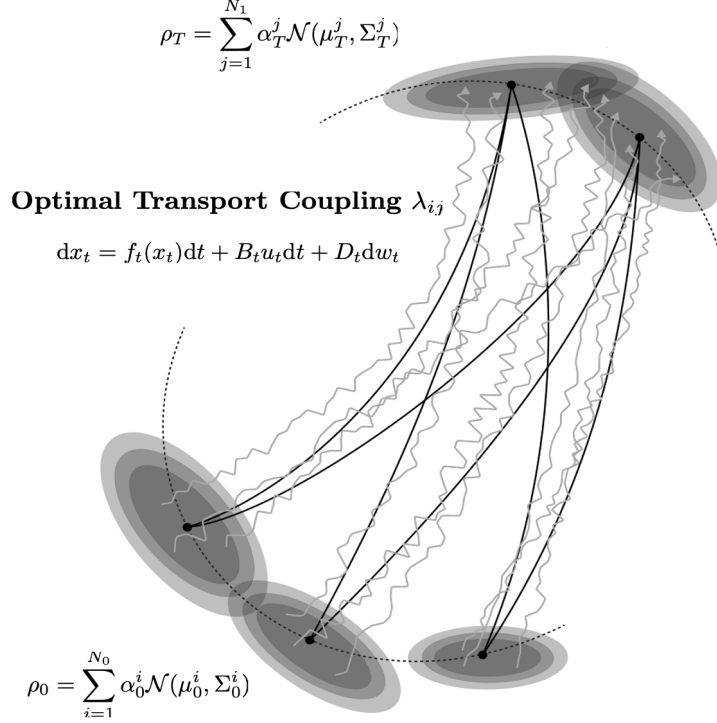


Figure 1 The problem of steering the initial distribution ρ_0 , modeled as Gaussian Mixture, of the state of a stochastic continuous-time non-linear system to a desired terminal distribution ρ_T (GMM), at a given stage $t = T$. Each ellipse in different intensity of gray represents a single Gaussian distribution, where a darker color highlights the region of more probability mass.

non-linear control law.

A. Multiple Distribution-to-Distribution Linearization

Let ρ_0 and ρ_T be the initial and final boundary distributions on \mathbb{R}^n . Since Gaussian mixture models are dense in the space of probability measures, any boundary distributions can be approximated arbitrarily well by GMMs [32]. To this end, we restrict our attention to the case where ρ_0 and ρ_T are some given GMMs and consider the problem

$$\min_{u \in \mathcal{U}} \mathbb{E}_{x_t} \left[\int_0^T \|u_t(x_t)\|^2 dt \right], \quad (14a)$$

$$\text{s.t. } dx_t = f_t(x_t)dt + B_t u_t dt + D_t dw_t, \quad (14b)$$

$$x_0 \sim \sum_{i=1}^{N_0} \alpha_0^i \mathcal{N}(\mu_0^i, \Sigma_0^i), \quad x_T \sim \sum_{j=1}^{N_1} \alpha_T^j \mathcal{N}(\mu_T^j, \Sigma_T^j). \quad (8c)$$

where the state is governed by the non-linear SDE (14b). Following [8, 13], we construct a policy similar to (9) by exploiting its mixture structure to linearize (14b) around different reference trajectories for each conditional policy.

Fig. 1 illustrates the high-level idea of this approach.

We now formally define the building blocks of the multiple linearization approach. For each component pair $(i, j) \in \{1, \dots, N_0\} \times \{1, \dots, N_1\}$, the *reference mean trajectory* $\mu_{t|ij}$ is defined as the solution of the *deterministic* open-loop optimal control problem

$$\min_{\bar{u}_{t|ij}} J_{ij} = \int_0^T \|\bar{u}_{t|ij}\|^2 dt \quad (15a)$$

$$\text{s.t. } \dot{\mu}_{t|ij} = f_t(\mu_{t|ij}) + B_t \bar{u}_{t|ij}, \quad (15b)$$

$$\mu_{0|ij} = \mu_0^i, \quad \mu_{T|ij} = \mu_T^j. \quad (15c)$$

where $\bar{u}_{t|ij}$ is the open-loop control obtained by solving the deterministic nonlinear program with boundary conditions fixed at the i -th initial and j -th terminal GMM component means.

With the optimal mean trajectory $\mu_{t|ij}$ and mean control $\bar{u}_{t|ij}$ solved, we evaluate the Jacobian matrix of the nonlinear drift term in (14b) around the reference mean trajectory using Equations (7b). The above procedure yields a set of matrix sequences $\{A_{t|ij} \in \mathbb{R}^{n \times n} : t \in [0, T]\}$, B_t and D_t .

Given the linearized system (7a), the associated (i, j) -OCS subpart is resolved as described in Section II.A, producing an optimal affine feedback law of the form

$$u_{t|ij}(x) = K_{t|ij}(x - \mu_{t|ij}) + \bar{u}_{t|ij}, \quad (16)$$

where $K_{t|ij} \in \mathbb{R}^{m \times n}$ is the optimal feedback gain controlling the covariance dynamics, and $\bar{u}_{t|ij}$ is the feedforward term steering the mean along the reference trajectory. The density of the (i, j) -th Gaussian bridge is given by

$$\rho_{t|ij} = \mathcal{N}(\mu_{t|ij}, \Sigma_{t|ij}), \quad (17)$$

and satisfies $\rho_{0|ij} = \mathcal{N}(\mu_0^i, \Sigma_0^i)$ and $\rho_{T|ij} = \mathcal{N}(\mu_T^j, \Sigma_T^j)$ by construction, while the mixture evolves according to (3b).

Repeating this procedure for each (i, j) of the $N_0 \times N_1$ subproblems allows us to define the necessary building blocks to compute the control law defined by (9) as a mixture of multiple linearizations, and hence we refer to this method as a *multiple linearization* approach. In particular, the conditional densities serve as the weighting kernels, while the final nonlinear controller is given by

$$u_t(x) = \sum_{i,j} \left[K_{t|ij}(x - \mu_{t|ij}) + \bar{u}_{t|ij} \right] \frac{\rho_{t|ij}(x) \lambda_{ij}}{\sum_{i',j'} \rho_{t|i'j'}(x) \lambda_{i'j'}}, \quad (18)$$

where the weights λ_{ij} are obtained by solving the linear program (11). This formulation ensures that, at any point x_t in the state-space, the overall control is a convex combination of the local affine policies (16), with each policy weighted

by the posterior probability that x_t was generated by the (i, j) -th Gaussian component $\rho_{t|ij}$ at time t .

We note that, in practice, this calculation is performed in a temporal discretization of the time horizon $[0, T]$. Since a sufficiently small time step introduces negligible discretization error, we carry out the analysis in continuous time and leave an inherently discrete-time analysis for future work.

B. Error Analysis and Density Characterization

We now evaluate the performance of the proposed multi-linearization approach in comparison to the single-linearization methods in [1, 20, 21]. Before formally assessing this claim, we first study an abstract problem from a function approximation perspective to understand how multiple linearizations can improve the accuracy of approximating a nonlinear function.

Consider a Gaussian mixture $\rho = \sum_i \alpha_i \mathcal{N}(\mu_i, \Sigma_i)$ with N components and mean $\mu = \sum_i \alpha_i \mu_i$. We consider two approximations of a differentiable function $f : \mathbb{R}^n \rightarrow \mathbb{R}^m$.

$$f_{\text{SL}}(x) = f(\mu) + \nabla f(\mu)(x - \mu), \quad (19)$$

$$f_{\text{ML}}(x) = \sum_i \frac{\alpha_i \mathcal{N}(x; \mu_i, \Sigma_i)}{\rho(x)} f_i(x), \quad (20)$$

where

$$f_i(x) \triangleq f(\mu_i) + \nabla f(\mu_i)(x - \mu_i) \quad (21)$$

denotes the linearization of f around the mean μ_i of the i -th mixture component.

In words, f_{SL} represents the single-linearization approximation around the global mean μ , while f_{ML} is a weighted average of linearizations around each component's mean μ_i .

We now state a result characterizing the upper bounds on the expected error of these two approximations.

Theorem 1. *Suppose the linearization error of f is uniformly quadratically bounded. Then, the upper bound on the expected error of the single linearization, i.e., $\mathbb{E}\|f - f_{\text{SL}}\|_2$, is equal or worse than the corresponding upper bound of the multiple linearization, i.e., $\mathbb{E}\|f - f_{\text{ML}}\|_2$.*

Proof. Since the linearization error of f is uniformly quadratically bounded, for all $x_0 \in \mathbb{R}^n$, we have

$$\|f(x) - \bar{f}_{x_0}(x)\|_2 \leq C \|x - x_0\|_2^2, \quad (22)$$

where $\bar{f}_{x_0}(x) \triangleq f(x_0) + \nabla f(x_0)(x - x_0)$ is the first-order approximation around x_0 , and C is a constant. For L -smooth functions, the quadratic error bound (22) follows from [[33], Eq.(8.3)] with $C = L/2$.

For the single linearization approximation (SL), the total expected approximation error is bounded as

$$\begin{aligned}\epsilon_{\text{SL}} &= \mathbb{E}_{\rho} \|f(x) - f_{\text{SL}}(x)\|_2 = \int_{\mathbb{R}^n} \|f(x) - f_{\text{SL}}(x)\|_2 \rho(x) \, dx \\ &\leq C \int_{\mathbb{R}^n} \|x - \mu\|_2^2 \rho(x) \, dx = C \, \text{tr}\Sigma,\end{aligned}\tag{23}$$

where Σ is the covariance of ρ .

Similarly, the multiple-linearization approximation (ML) yields the following upper bound on the expected error

$$\epsilon_{\text{ML}} = \int_{\mathbb{R}^m} \|f(x) - f_{\text{ML}}(x)\|_2 \rho(x) \, dx,\tag{24a}$$

$$\leq \sum_{i=1}^N \alpha^i \int_{\mathbb{R}^m} \|f(x) - f_i(x)\|_2 \mathcal{N}(x; \mu_i, \Sigma_i) \, dx\tag{24b}$$

$$\leq \sum_{i=1}^N \alpha^i C \int_{\mathbb{R}^n} \|x - \mu_i\|_2^2 \mathcal{N}(x; \mu_i, \Sigma_i) \, dx\tag{24c}$$

$$= C \sum_i \alpha^i \text{tr}\Sigma_i,\tag{24d}$$

where (24b) is from Jensen's inequality and (24d) follows from (22). Using the variance decomposition, we obtain

$$\Sigma = \sum_i \alpha_i \Sigma_i + \sum_i \alpha_i (\mu_i - \mu)(\mu_i - \mu)^\top.\tag{25}$$

Taking the trace on both sides of (25) leads to

$$\text{tr}\Sigma = \sum_i \alpha^i \text{tr}\Sigma_i + \sum_i \alpha^i \|\mu_i - \mu\|_2^2,\tag{26}$$

which implies $\text{tr}\Sigma \geq \sum_i \alpha^i \text{tr}\Sigma_i$

By defining the upper bounds as $\epsilon_{\text{SL}}^{\text{ub}} = C \, \text{tr}\Sigma_t$ and $\epsilon_{\text{ML}}^{\text{ub}} = C \sum_{i=1}^N \alpha^i \text{tr}\Sigma_t^i$, we have $\epsilon_{\text{SL}}^{\text{ub}} \geq \epsilon_{\text{ML}}^{\text{ub}}$. \square

Unfortunately, we note that an improved upper bound on the linearization error between the multi and single linearization techniques does not, in general, imply better approximation accuracy, since the derived upper bounds might not be tight. A natural question, therefore, is under what conditions on f can we obtain a stronger result. It turns out that the convexity or concavity of the components of the vector field f is sufficient to prove strictly better approximation accuracy between the multi and single linearization approaches. We establish this in Theorem 2, after first proving a necessary lemma. In the following, to facilitate a component-wise analysis, we will compare the linearization accuracy through the expected 1-norm error, denoted with $\|\cdot\|$.

Lemma 1. *Consider the i -th component of the GMM in Equation (21) and assume each component $f^{(k)} : \mathbb{R}^n \rightarrow \mathbb{R}$,*

$k \in \{1, \dots, m\}$ of the vector field f , is either globally strictly convex or globally strictly concave. Then for any $a \in \mathbb{R}^n$:

$$\int \|f(x) - f_i(x)\| \mathcal{N}(\mu_i, \Sigma_i) dx \leq \int \|f(x) - f_a(x)\| \mathcal{N}(\mu_i, \Sigma_i) dx. \quad (27)$$

Proof. Consider a single component $f^{(k)}$ with linearization $f_a^{(k)}(x) = f^{(k)}(a) + \nabla f^{(k)}(a)^T(x - a)$. Define

$$g(a) = \mathbb{E}_{x \sim \mathcal{N}(\mu_i, \Sigma_i)} \left[|f^{(k)}(x) - f_a^{(k)}(x)| \right]. \quad (28)$$

Convex case: Since $f^{(k)}(x) \geq f_a^{(k)}(x)$ for all $x, a \in \mathbb{R}^n$, we can remove the absolute value and obtain

$$\begin{aligned} g(a) &= \mathbb{E}_x [f^{(k)}(x) - f_a^{(k)}(a) - \nabla f^{(k)}(a)^T(x - a)] \\ &= \mathbb{E}_x [f^{(k)}(x)] - f_a^{(k)}(a) - \nabla f^{(k)}(a)^T(\mathbb{E}[x] - a) \\ &= \mathbb{E}_x [f^{(k)}(x)] - f_a^{(k)}(a) - \nabla f^{(k)}(a)^T(\mu_i - a) \geq 0 \end{aligned}$$

With strict convexity, one can further show that $g(a^*) = 0$ only when $a^* = \mu_i$. Formally, setting $\nabla_a g(a^*) = 0$ yields $H_{f^{(k)}}(a)(\mu_i - a^*) = 0$. Due to strict convexity, we have $H_{f^{(k)}} \succ 0$, and thus $a^* = \mu_i$.

Concave case: We have $f^{(k)}(x) \leq f_a^{(k)}(x)$ for all $x, a \in \mathbb{R}^n$. Through a similar argument, we have $g(a) \geq 0$ with equality attained only at $a^* = \mu_i$.

For the vector case, the 1-norm yields

$$\begin{aligned} \int \|f(x) - f_{\mu_i}(x)\| \mathcal{N}(\mu_i, \Sigma_i) dx &= \sum_{k=1}^m \int |f^{(k)}(x) - f_{\mu_i}^{(k)}(x)| \mathcal{N}(\mu_i, \Sigma_i) dx \\ &\leq \sum_{k=1}^m \int |f^{(k)}(x) - f_a^{(k)}(x)| \mathcal{N}(\mu_i, \Sigma_i) dx \\ &= \int \|f(x) - f_a(x)\| \mathcal{N}(\mu_i, \Sigma_i) dx. \end{aligned}$$

□

Theorem 2. Let $f : \mathbb{R}^n \rightarrow \mathbb{R}^m$ be a C^1 function, with Lipschitz derivative. Let f_{SL}, f_{ML} be defined as in (19), (20), respectively. If f satisfies the conditions of Lemma 1 for each component k and the means of the GMM components are not identical, then $\mathbb{E}\|f - f_{SL}\| > \mathbb{E}\|f - f_{ML}\|$.

Proof. In single linearization, we linearize around the global mean of ρ , i.e., $\mu = \sum_i \alpha_i \mu_i$. The total expected approximation error is the integral

$$\epsilon_{SL} = \int \|f(x) - f_{SL}(x)\| \rho(x) dx. \quad (29)$$

Since the density is a mixture $\rho(x) = \sum_{i=1}^N \alpha_i \mathcal{N}(\mu_i, \Sigma_i)$, we can decompose this expected error as:

$$\epsilon_{\text{SL}} = \sum_{i=1}^N \alpha_i \int \|f(x) - f_{\text{SL}}(x)\| \mathcal{N}(\mu_i, \Sigma_i) dx. \quad (30)$$

Similarly, the Multiple Linearization (ML) approximation yields the following expected error:

$$\epsilon_{\text{ML}} = \int \|f(x) - f_{\text{ML}}(x)\| \rho(x) dx, \quad (31a)$$

$$\leq \sum_{i=1}^N \alpha_i \int \|f(x) - f_i(x)\| \mathcal{N}(\mu_i, \Sigma_i) dx, \quad (31b)$$

where (31b) follows from Jensen's inequality and the convexity of the norm.

By our assumption on f and Lemma 1, the expected linearization error for any specific component i is minimized when linearizing around its own mean μ_i . Therefore, the error of the global linearization f_{SL} (which is centered at μ) can only yield an equal or worse expected error for that component:

$$\int \|f(x) - f_i(x)\| \mathcal{N}(\mu_i, \Sigma_i) dx \leq \int \|f(x) - f_{\text{SL}}(x)\| \mathcal{N}(\mu_i, \Sigma_i) dx. \quad (32)$$

Substituting (32) into (31b) and comparing with (30) yields the following relation between the actual expected errors:

$$\epsilon_{\text{ML}} \leq \sum_{i=1}^N \alpha_i \int \|f(x) - f_{\text{SL}}(x)\| \mathcal{N}(\mu_i, \Sigma_i) dx = \epsilon_{\text{SL}}. \quad (33)$$

Furthermore, equality holds only when the global mean—at which f_{SL} is linearized—coincides with the mean of each individual GMM component. As the component means are assumed to be not identical, the inequality is strict. \square

We now return to Problem (14). We verify that, under the multiple-linearization policy, the mixture density ρ_t satisfies an FPK equation (cf. Section II.D) whose drift approximates the true nonlinear drift f_t . Specifically, consider the FPK equation corresponding to the (i, j) -linearization, with drift $\bar{f}_{t|ij}(x) = f_t(\mu_{t|ij}) + A_{t|ij}(x - \mu_{t|ij})$, given by

$$\frac{\partial \rho_{t|ij}}{\partial t} + \nabla \cdot (\rho_{t|ij} (\bar{f}_{t|ij} + B_t u_{t|ij})) - \frac{1}{2} \text{tr}(DD^\top \nabla^2 \rho_{t|ij}) = 0, \quad (34)$$

where $u_{t|ij}$ solves the (i, j) -OCS subproblem. Multiplying by λ_{ij} and summing over all (i, j) pairs yields

$$\frac{\partial \rho_t}{\partial t} + \nabla \cdot [(f_{\text{ML}} + B_t u_t) \rho_t] - \frac{1}{2} \text{tr}(DD^\top \nabla^2 \rho_t) = 0, \quad (35)$$

where,

$$f_{\text{ML}} = \sum_{ij} \bar{f}_{t|ij} \frac{\lambda_{ij} \rho_{t|ij}}{\rho_t}, \quad (36)$$

with $\rho_t = \sum_{ij} \lambda_{ij} \rho_{t|ij}$, and u_t is defined by (18). Equation (35) shows that if the system dynamics were evolving according to f_{ML} , the controller (18) would indeed transport the GMM ρ_0 to ρ_T *exactly*, serving as a foundation for our motivation. Furthermore, since according to Theorems 1, 2, f_{ML} is a better approximation of the nonlinear function f compared to a single linearization, we expect the true ρ_T to be closer to the terminal GMM, compared to a linear controller.

Finally, we remark that the component-wise convexity requirement to guarantee improved approximation accuracy through Theorem 2 might be too strong for many practical problems, including our case study scenario relevant to spacecraft navigation in the following section. Empirically, we observe that the ML method continues to outperform SL even when the convexity conditions are not satisfied, as demonstrated in our numerical simulations.

IV. Numerical Simulation

We evaluate the efficacy of the proposed *multiple distribution-to-distribution linearization* method using the Earth-Mars rendezvous scenario presented in [21] under nonlinear orbital dynamics and non-Gaussian state uncertainty.

A. Modeling of the dynamics

The dynamics are expressed in a Sun-centered inertial frame restricted to the ecliptic plane (2D). Assume the spacecraft has approximately constant mass and leaves Earth with zero hyperbolic excess velocity. The physical state is defined by position and velocity expressed in Cartesian components, namely $r_t = [x_t, y_t]^\top$, $v_t = [v_t^x, v_t^y]^\top$. Assume the spacecraft is modeled as a point mass and the applied control is the acceleration provided by the thrusters $u_t = [u_t^x, u_t^y]^\top$. In state-space form, the dynamics can be written as:

$$\dot{x}_t = \begin{bmatrix} v_t \\ -\frac{\mu_\odot}{\|r_t\|^3} r_t \end{bmatrix} + \begin{bmatrix} 0 \\ I \end{bmatrix} u_t + \begin{bmatrix} 0 \\ g_v I \end{bmatrix} w_t, \quad (37)$$

where $x_t = [x, y, v_x, v_y]^\top$. Note that the final time T is fixed and known, and the Sun's gravity and the noise are the only external forces acting on the system. All variables and parameters are scaled to reduce disparities in their orders of magnitude, which is essential for the convergence of the algorithm. Scaling is performed relative to the astronomical unit (AU) and days. The related linearized representation is:

$$A_t = \frac{\partial f}{\partial x} = \begin{bmatrix} 0_{2 \times 2} & I_{2 \times 2} \\ A_{vr} & 0_{2 \times 2} \end{bmatrix}, B_t = \begin{bmatrix} 0_{2 \times 2} \\ I_{2 \times 2} \end{bmatrix}, D_t = \begin{bmatrix} 0_{2 \times 2} \\ g_v I_{2 \times 2} \end{bmatrix},$$

$$\text{where } A_{vr} = \mu_{\odot} \begin{bmatrix} \frac{3x^2 - \|r\|^2}{\|r\|^5} & \frac{3xy}{\|r\|^5} \\ \frac{3xy}{\|r\|^5} & \frac{3y^2 - \|r\|^2}{\|r\|^5} \end{bmatrix}.$$

In practice, we replace the process noise covariance $D_t D_t^T$, with

$$\hat{\Sigma}_d = \begin{bmatrix} 0_{2 \times 2} & 0_{2 \times 2} \\ 0_{2 \times 2} & g_v I_{2 \times 2} \end{bmatrix} + \varepsilon I_{4 \times 4}, \quad (38)$$

where $\varepsilon > 0$ models an artificial noise induced by the linearization.

The nonlinear program (NLP) used to compute the open-loop reference is solved using Sequential Least Squares Quadratic Programming (SLSQP). To provide an accurate initial guess, we adopt a Hohmann transfer estimate, motivated by the well-known sensitivity of this class of algorithms to initialization. Finally, the $N_0 \times N_1$ OCS subproblems are solved using MOSEK [34].

Table 1 Initial values and simulation parameters.*

Parameter	Symbol	Value
<i>Simulation Parameters</i>		
Init. Components	N_0	3
Target Components	N_1	2
Time Nodes	N	101
Diffusion Scale	ε^2	$10^{-7} \text{diag}([0.05, 0.05, 0.1, 0.1])$
Noise Intensity	g_v	$10^{-4} \text{ m/s}^{3/2}$
Sun Grav. Param.	μ_{\odot}	$2.9591 \times 10^{-4} \text{ AU}^3/\text{day}^2$
<i>Boundary Conditions – Case I</i>		
Init. Covariances	$\Sigma_{i,0}$	$\text{diag}(4.5 \times 10^{-9}, 4.5 \times 10^{-9}, 3.5 \times 10^{-9}, 3.5 \times 10^{-9})$
Target Covariances	$\Sigma_{j,T}$	$\text{diag}(4.5 \times 10^{-6}, 4.5 \times 10^{-6}, 3.5 \times 10^{-8}, 3.5 \times 10^{-8})$
Weights	α_0, α_1	$1/N_0, 1/N_1$
<i>Boundary Conditions – Case II</i>		
Init. Mean	μ_0	$(-0.9405, -0.3450) \text{ AU}$ $(9.7746, -28.078) \text{ km/s}$
Target Mean	μ_1	$(-1.1543, 1.1829) \text{ AU}$ $(-16.427, -14.861) \text{ km/s}$
Init. Covariance	Σ_0	$\text{diag}(10^{-3}, 10^{-3}, 10^{-7}, 10^{-7})$
Target Covariance	Σ_T	$\text{diag}(10^{-3}, 10^{-3}, 10^{-7}, 10^{-7})$

*Reference scales and simulation parameters are common to both cases.

To properly evaluate the efficacy of the proposed method, Monte Carlo simulations were conducted considering two

primary guidance policies: SL and ML. In the following two subsections, we present two different variations of the problem described here.

B. Case I: Multi-Modal Boundary Distributions

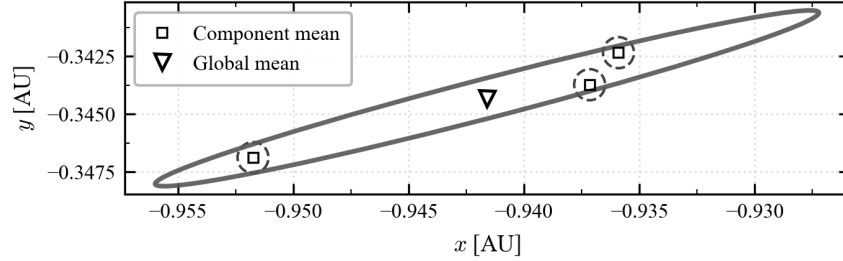


Figure 2 Initial multi-modal distribution ρ_0 . Covariance ellipses associated with the Gaussian components ($i = 1, 2, 3$) are computed at the two-standard-deviation level and scaled by a factor of 5 for clarity.

The first case of interest we investigate is the behavior of both algorithms under multimodal distributions. This corresponds to a situation where multiple starting points and multiple targets can be reached with a prescribed probability and accuracy. Formally, this translates to a case where we have N_0 Gaussian components, each representing a possible initial state, with an associated covariance describing the uncertainty around that specific state. A similar interpretation can be given for the multiple-arrival condition. To this end, the initial and final distributions ρ_0 and ρ_T are chosen to be composed of three (Figure 2) and two (Figure 4) isolated Gaussian components, respectively, such that their corresponding covariance ellipses are far from intersecting.

The ML approach exploits the superposition of local affine policies to effectively capture the underlying local nonlinearities and sparse concentration of the distribution. In contrast, the SL approach solves a single mean-to-mean problem, from the initial global mean to the final global mean, and is therefore unable to capture the separation of the probability mass, whereas ML successfully addresses this feature. The obtained solutions are presented in Figures 3 and 4.

C. Case II: Exploitation of Multiple Linearizations

Consider a different scenario where the marginal constraints correspond to distributions with large covariances. Specifically, we consider the distributions in Figures 5 and 7, with nominal values given in Table 1. By artificially fitting a GMM to ρ_0 and ρ_T , we can construct a more accurate approximation of the nonlinear controller, by leveraging the concept of multiple linearizations. We evaluate this claim in terms of the resulting control effort of the proposed approach, calculated through Monte Carlo realizations, against the control cost of a single linearization. While both methods converge to the desired target, the ML-based approach achieves the solution at a significantly lower cost J_{ctrl} .

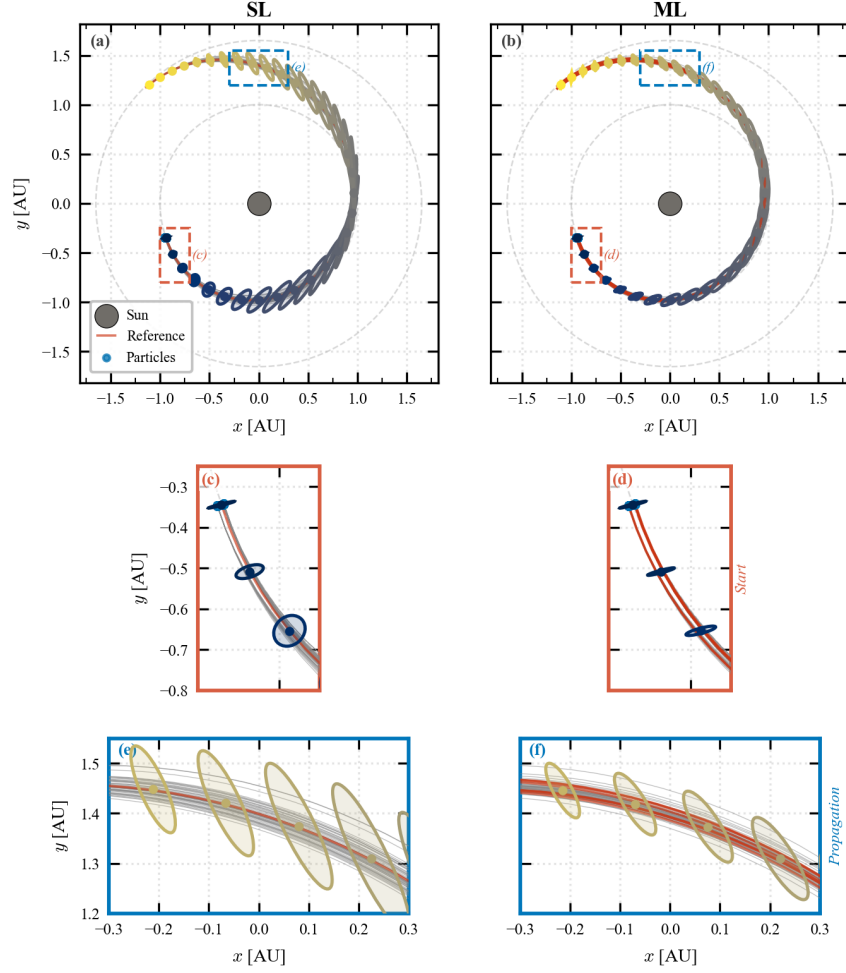


Figure 3 Case I: position evolution under SL (a) and ML (b) policies. Top row depicts phase-space trajectories from $t = 0$ (dark blue) to $t = T$ (yellow), showing the evolution of 200 Monte Carlo samples (gray). Panels (c)–(d) illustrate the propagation of the initial samples drawn from ρ_0 , shown in light blue. The red curves denote the reference trajectories (bridges). (e)–(f) provide zoomed-in views highlighting an intermediate time window, illustrating tighter covariance control under ML. The ellipses represent 3σ confidence regions computed from the empirical distribution.

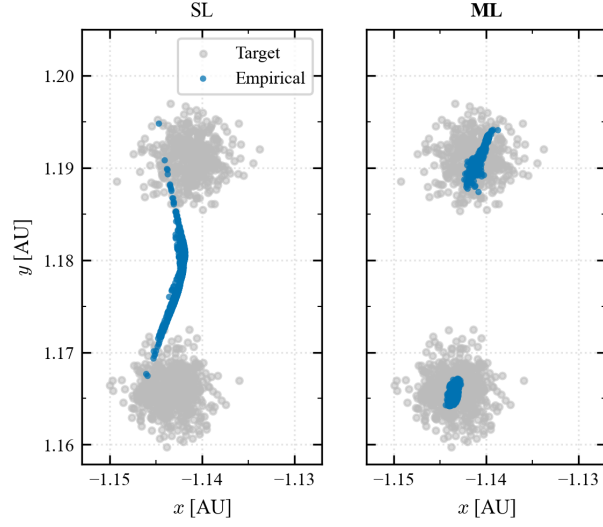


Figure 4 Case I: terminal distribution matching.

Let the Monte Carlo cost estimation be defined as

$$J_{\text{ctrl}} = \frac{1}{N_p} \sum_{p=1}^{N_p} \sum_{k=1}^N \|u_k(x_k^{(p)})\|^2 \Delta t_k, \quad (39)$$

where N_p is the number of particles.

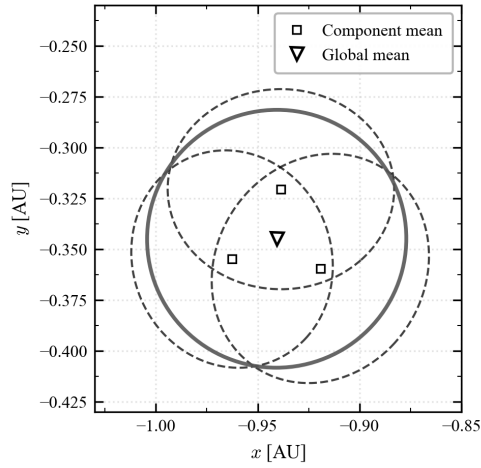


Figure 5 Initial close-to-Gaussian distribution ρ_0 . Covariance ellipses are computed at the 2σ level.

The ML approach achieves tighter distribution control throughout the transfer.

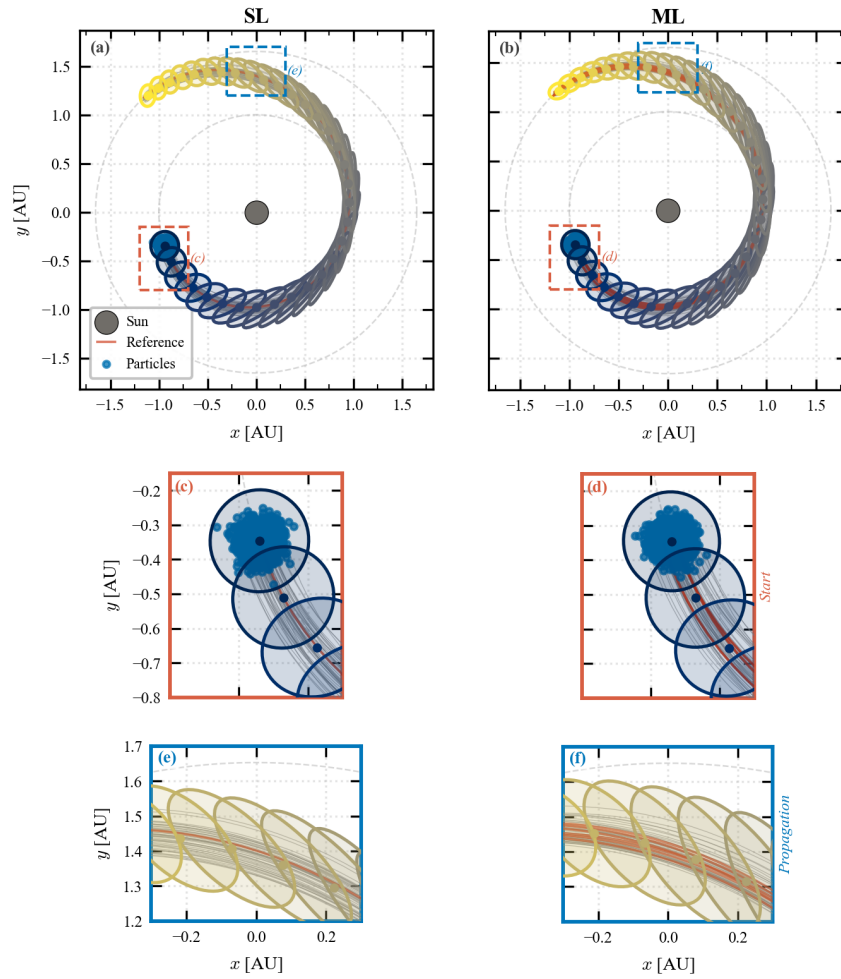


Figure 6 Case II: position evolution under SL (a) and ML (b) policies. Layout as in Figure 3.

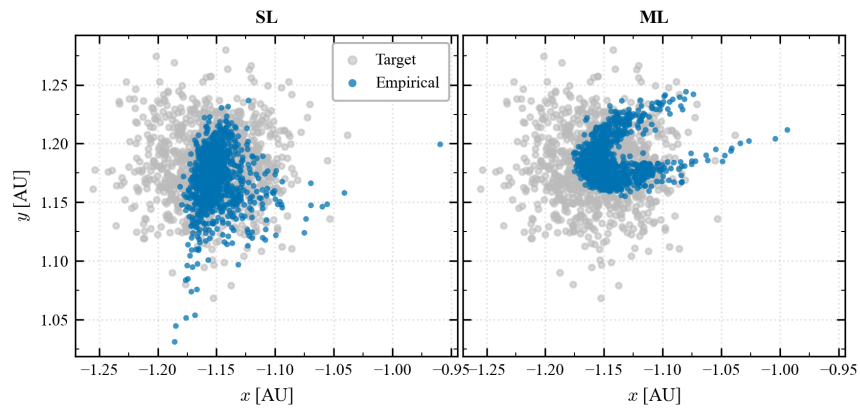


Figure 7 Case II: terminal distribution matching.

Table 2 Monte Carlo estimation Control cost comparison for Single vs Multiple Linearization. Note: J_{ctrl} is reported in units of 10^{-7} , while Sliced W_2 is reported in units of 10^{-3} . (I) and (II) denote Case I and Case II, respectively.

Mode	J_{ctrl} (I)	J_{ctrl} (II)	Sliced W_2 (I)	Sliced W_2 (II)
SL	1.82695	1.95150	4.44686	13.5541
ML	1.65157	1.64075	1.25304	12.4214

D. Metrics of Comparison

The Earth-to-Mars interplanetary transfer introduces coupled non-linear gravity dynamics according to (37), resulting in a state distribution that heavily strays from the initial Gaussian assumptions over the integration horizon. It is evident that the Single Linearization (SL) policy, which relies on an affine approximation centered around the aggregate global mean of the GMM, struggles to accurately capture the structural dispersion of the probability mass. To quantify terminal distribution matching, we report the Sliced Wasserstein-2 (Sliced W_2) distance, a tractable approximation of the Wasserstein-2 distance obtained by averaging one-dimensional optimal transport costs over random projections [35]; a lower W_2 value indicates that the empirical terminal distribution of the Monte Carlo samples is closer to the desired target ρ_T .

The generated feedback control commands manifest a 10.62% (Case I) and 18.94% (Case II) higher cost with respect to the ML case, while also yielding a larger Sliced W_2 distance, confirming that SL produces a less accurate terminal distribution match. The quantitative metrics obtained are summarized in Table 2.

V. Conclusions

This paper introduced a multiple linearization approach for nonlinear stochastic density steering problems. By decomposing the problem into a mixture of local OCS subproblems, each linearizing the original problem around a different mean trajectory, the proposed method accurately handles multi-modal uncertainty in highly nonlinear regimes. Theoretical analysis demonstrated that multiple linearizations provide tighter error bounds than single linearization when steering multi-modal distributions. Numerical results on the Earth-to-Mars transfer problem validated this finding, showing cost reduction compared to single linearization while maintaining terminal distribution constraints.

Acknowledgment

The authors express their thanks to Luigi Tesio for his assistance in designing Figure 1. George Rapakoulias acknowledges support from the A. Onassis Foundation.

References

- [1] Ridderhof, J., Pilipovsky, J., and Tsiotras, P., “Chance-constrained covariance control for low-thrust minimum-fuel trajectory optimization,” *2020 AAS/AIAA Astrodynamics Specialist Conference*, 2020, pp. 9–13.
- [2] Exarchos, I., and Theodorou, E. A., “Stochastic optimal control via forward and backward stochastic differential equations and importance sampling,” *Automatica*, Vol. 87, 2018, pp. 159–165.
- [3] Chen, Y., Georgiou, T. T., and Pavon, M., “Controlling uncertainty,” *Control Systems Magazine*, Vol. 41, No. 4, 2021, pp. 82–94.
- [4] Caluya, K. F., and Halder, A., “Wasserstein proximal algorithms for the Schrödinger bridge problem: Density control with nonlinear drift,” *Transactions on Automatic Control*, Vol. 67, No. 3, 2021, pp. 1163–1178.
- [5] Pilipovsky, J., and Tsiotras, P., “DUST: A Framework for Data-Driven Density Steering,” *arXiv preprint arXiv:2408.02777*, 2024.
- [6] Saravanos, A. D., Li, Y., and Theodorou, E. A., “Distributed Hierarchical Distribution Control for Very-Large-Scale Clustered Multi-Agent Systems,” *Robotics: Science and Systems XIX*, Daegu, Republic of Korea, 2023.
- [7] Chen, Y., Georgiou, T. T., and Pavon, M., “Stochastic control liaisons: Richard Sinkhorn meets Gaspard Monge on a Schrödinger bridge,” *SIAM Review*, Vol. 63, No. 2, 2021, pp. 249–313.
- [8] Rapakoulias, G., Pedram, A. R., Liu, F., Zhu, L., and Tsiotras, P., “Go With the Flow: Fast Diffusion for Gaussian Mixture Models,” *The Thirty-ninth Annual Conference on Neural Information Processing Systems*, 2025.
- [9] Chen, Y., Georgiou, T. T., and Pavon, M., “Optimal transport over a linear dynamical system,” *Transactions on Automatic Control*, Vol. 62, No. 5, 2016, pp. 2137–2152.
- [10] Mei, Y., Al-Jarrah, M., Taghvaei, A., and Chen, Y., “Flow matching for stochastic linear control systems,” *Proceedings of the 7th Annual Learning for Dynamics & Control Conference*, Vol. 283, PMLR, 2025, pp. 484–496.
- [11] Liu, G.-H., Chen, T., So, O., and Theodorou, E., “Deep Generalized Schrödinger Bridge,” *Advances in Neural Information Processing Systems*, Vol. 35, Curran Associates, Inc., Louisiana, LA, 2022, pp. 9374–9388.
- [12] Chen, Y., Georgiou, T. T., and Pavon, M., “Steering the distribution of agents in mean-field games system,” *Journal of Optimization Theory and Applications*, Vol. 179, 2018, pp. 332–357.
- [13] Rapakoulias, G., Reza Pedram, A., and Tsiotras, P., “Steering Large Agent Populations Using Mean-Field Schrödinger Bridges With Gaussian Mixture Models,” *IEEE Control Systems Letters*, Vol. 9, 2025, pp. 1760–1765. <https://doi.org/10.1109/LCSYS.2025.3581859>.
- [14] Chen, Y., Georgiou, T. T., and Pavon, M., “Optimal steering of a linear stochastic system to a final probability distribution, Part II,” *Transactions on Automatic Control*, Vol. 61, No. 5, 2015, pp. 1170–1180.

- [15] Bakolas, E., “Optimal covariance control for discrete-time stochastic linear systems subject to constraints,” *Proceedings of the 55th IEEE Conference on Decision and Control (CDC)*, IEEE, 2016, pp. 1153–1158.
- [16] Liu, F., Rapakoulias, G., and Tsiotras, P., “Optimal Covariance Steering for Discrete-Time Linear Stochastic Systems,” *Transactions on Automatic Control*, 2024, pp. 1–16. <https://doi.org/10.1109/TAC.2024.3472788>.
- [17] Rapakoulias, G., and Tsiotras, P., “Discrete-Time Optimal Covariance Steering via Semidefinite Programming,” *62nd Conference on Decision and Control*, Singapore, 2023, pp. 1802–1807. <https://doi.org/10.1109/CDC49753.2023.10384118>.
- [18] Chen, Y., Georgiou, T. T., and Pavon, M., “Optimal Steering of a Linear Stochastic System to a Final Probability Distribution, Part I,” *Transactions on Automatic Control*, Vol. 61, No. 5, 2015, pp. 1158–1169.
- [19] Ito, K., and Kashima, K., “Maximum entropy density control of discrete-time linear systems with quadratic cost,” *IEEE Transactions on Automatic Control*, Vol. 70, No. 5, 2024, pp. 3024–3039.
- [20] Ridderhof, J., Okamoto, K., and Tsiotras, P., “Nonlinear uncertainty control with iterative covariance steering,” *2019 IEEE 58th Conference on Decision and Control (CDC)*, IEEE, 2019, pp. 3484–3490.
- [21] Benedikter, B., Zavoli, A., Wang, Z., Pizzurro, S., and Cavallini, E., “Convex Approach to Covariance Control with Application to Stochastic Low-Thrust Trajectory Optimization,” *Journal of Guidance, Control, and Dynamics*, Vol. 45, No. 11, 2022, pp. 2061–2075. <https://doi.org/10.2514/1.G006806>, URL <https://arc.aiaa.org/doi/10.2514/1.G006806>.
- [22] Kumagai, N., and Oguri, K., “Robust cislunar low-thrust trajectory optimization under uncertainties via sequential covariance steering,” *Journal of Guidance, Control, and Dynamics*, Vol. 48, No. 12, 2025, pp. 2725–2743.
- [23] Kumagai, N., and Oguri, K., “Hands-Off Covariance Steering: Inducing Feedback Sparsity via Iteratively Reweighted $\ell_{1,p}$ Regularization,” *2025 IEEE 64th Conference on Decision and Control (CDC)*, IEEE, 2025, pp. 3560–3565.
- [24] Berner, J., Richter, L., and Ullrich, K., “An optimal control perspective on diffusion-based generative modeling,” *arXiv preprint arXiv:2211.01364*, 2022.
- [25] Domingo-Enrich, C., et al., “Stochastic Optimal Control Matching,” *Advances in Neural Information Processing Systems*, Vol. 37, 2024.
- [26] Balci, I. M., and Bakolas, E., “Exact SDP formulation for discrete-time covariance steering with Wasserstein terminal cost,” *arXiv preprint arXiv:2205.10740*, 2022.
- [27] Mao, Y., Szmuk, M., and Açikmeşe, B., “Successive convexification of non-convex optimal control problems and its convergence properties,” *2016 IEEE 55th Conference on Decision and Control (CDC)*, IEEE, 2016, pp. 3636–3641.
- [28] Balci, I. M., and Bakolas, E., “Density steering of Gaussian mixture models for discrete-time linear systems,” *2024 American Control Conference (ACC)*, 2024, pp. 3935–3940.

- [29] Kumagai, N., and Oguri, K., “Chance-Constrained Gaussian Mixture Steering to a Terminal Gaussian Distribution,” *63rd Conference on Decision and Control*, Milan, 2024, pp. 2207–2212.
- [30] Rapakoulias, G., Liu, F., and Tsiotras, P., “Schrödinger Bridges and Density Steering Problems for Gaussian Mixtures Models in Discrete-Time,” *arXiv preprint arXiv:2604.01144*, 2026.
- [31] Särkkä, S., and Solin, A., *Applied stochastic differential equations*, Vol. 10, Cambridge University Press, 2019.
- [32] Maz’ya, V. G., and Schmidt, G., *Approximate Approximations*, Mathematical Surveys and Monographs, Vol. 141, American Mathematical Society, Providence, Rhode Island, 2007.
- [33] Nocedal, J., and Wright, S., *Numerical Optimization*, 2nd ed., Springer Science & Business Media, New York, 2006.
- [34] MOSEK ApS, “MOSEK modeling cookbook,” , 2020.
- [35] Bonneel, N., Rabin, J., Peyré, G., and Pfister, H., “Sliced and radon Wasserstein barycenters of measures,” *Journal of Mathematical Imaging and Vision*, Vol. 51, No. 1, 2015, pp. 22–45.